This is the peer-reviewed, final accepted version for American Mineralogist, published by the Mineralogical Society of America.
The published version is subject to change. Cite as Authors (Year) Title. American Mineralogist, in press.
DOI: https://doi.org/10.2138/am-2022-8799. http://www.minsocam.org/

Revision 1

Reaction between volatile-bearing eclogite and harzburgite as a function of degree of interaction: experimental constraints at 4 GPa

ELAZAR, ODED[1] AND KESSEL, RONIT[1,*]

[1]Fredy and Nadin Herrmann Institute of Earth Sciences, The Hebrew University of Jerusalem, Jerusalem 91904, Israel

Corresponding author: ronit.kessel@mail.huji.ac.il

ABSTRACT

The mantle is known to be heterogeneous, mainly composed of peridotite and eclogite. Eclogite-derived hydrous melts may interact with harzburgite at the slab-mantle interface in subduction zones or in the sub-continental lithospheric mantle. In this study, such interactions were simulated by performing hybrid experiments in which a layer of eclogite has been juxtaposed to a layer of harzburgite, in the presence of H_2O-CO_2 at 4 GPa and 1200^{o}C, conditions where eclogite is super-solidus while harzburgite is sub-solidus. A diamond trap was placed in between the two layers in order to trap the fluid or melt phase, allowing direct determination of their composition. The multi-anvil was rotated in different frequencies in order to examine the effect of increasing degree of interaction on the melt composition as well as the mineral compositions. The interaction of eclogite-derived hydrous melt and harzburgite results in a reaction layer at the interface between the two lithologies, composed of opx and garnet. The harzburgite above the reaction layer is metasomatized, containing various

amounts of olivine, opx, cpx and garnet. The eclogitic melt is modified during this interaction. With increasing interaction, a thicker reaction layer is formed. Both the eclogitic and the peridotitic garnet compositions approach each other and become intermediate between the composition of the garnet in the eclogite+H_2O+CO_2 system and the garnet in the harzburgite+H_2O+CO_2 system at these conditions. The Mg# of the peridotitic olivine and opx decreases with increasing interaction. The initial basaltic melt in equilibrium with eclogitic garnet is metaluminous, turning to a peralkaline melt with increasing interaction with the harzburgite. The metasomatizing effect of the eclogite-derived hydrous melt on the harzburgite is observed by increasing the mode of the peridotitic opx, cpx and garnet at the expense of peridotitic olivine and eclogitic garnet. Slight increase in melt fraction occurs as well. This interaction also results in a gradient in the log$f$$O_2$. Relatively more oxidizing conditions occur near the reaction layer, becoming more reduced into the peridotite suggesting that the reaction zones act as partial barriers for the melt to travel through the peridotite. Increased interaction leads to higher log$f$$O_2$ values. These experiments demonstrate the influence of the degree of interaction on the range of melt compositions found in volcanic arcs as well as the degree of metasomatism in the mantle found in the sub continental lithospheric mantle.

INTRODUCTION

Heterogeneity in the Earth's mantle has been vastly documented through numerous mineralogical, geochemical, and experimental studies of rocks and magmas (e.g., Allègre and Turcotte 1986; Qian et al. 2022; Qiao et al. 2023; Sobolev et al. 2005; Stachel et al. 2018; Stracke 2012 among others). Geophysical studies have also revealed significant variations in the seismic velocity and density of the mantle, indicating the existence of different domains at

46 depth (e.g., Schaffer and Lebedev 2013). Subducted oceanic crust is the most dominant form
47 of heterogeneity in the mantle. For example, eclogitic lenses and veins are known to be
48 embedded in the peridotitic mantle (e.g., Helffrich and Wood 2001; Hofmann 1988; Hofmann
49 1997; Jackson and Dasgupta 2008; Lassiter and Hauri 1998). Melting of hydrothermally
50 altered eclogite occurs at significantly lower temperatures than hydrous or dry peridotite at the
51 same pressure (Dasgupta et al. 2005; Dasgupta et al. 2004; Eggler 1978). Hence, a
52 heterogeneous mantle zone consisting of both peridotite and hydrous eclogite may result in
53 the formation of eclogite-derived hydrous melt interacting with the host peridotite. Such
54 interactions may occur in young subduction zones, where the hot oceanic slab undergoes
55 melting. The eclogite-derived hydrous melt rises into and interacts with the depleted
56 peridotitic mantle just above the subducting slab. In the sub continental lithospheric mantle,
57 eclogite-derived hydrous melt may infiltrate and interact with the surrounding harzburgite
58 (Stachel and Harris 2008).

59 Evidence for the interaction of eclogite-derived hydrous melt and peridotite is abundant in
60 ophiolites, peridotite massifs and xenoliths (e.g., Kelemen et al. 1990; Wang et al. 2016). For
61 example, the formation of orthopyroxenite veins in peridotite, found in cratonic (e.g., Bell et
62 al. 2005; Boyd 1989; Kelemen et al. 1992; Kelemen et al. 1998) and orogenic peridotites
63 (e.g., Malaspina et al. 2006), is typically attributed to the infiltration of eclogite-derived
64 hydrous melt into the host peridotite. In places, opx veins are associated with hydrous
65 minerals such as amphibole and phlogopite (Xu et al. 2020), supporting the hydrous nature of
66 the interaction. The thickness of such veins can range from a few centimeters to several
67 meters (i.e., Le Roex et al. 2014; Wang et al. 2016; Xu et al. 2008). Arc lavas have a wide
68 range of compositions, from silica saturated to silica undersaturated basalts to dacite.

Chemical and isotopic compositions support the idea that many arc magmas have complex multi-source petrogenesis (Atherton and Tarney, 1979; DePaolo, 1981; Hildreth, 1981; Kay, 1980). Reaction of eclogite-derived hydrous melt and peridotite has also been advocated to result in the formation of Mg-rich basalts and andesites in volcanic arcs (e.g., Rapp et al. 1999; Yogodzinski et al. 1994).

The infiltration of eclogite-derived melt into a peridotite leads to changes in the chemistry of the peridotite minerals (cryptic metasomatism) or the formation of new minerals (modal metasomatism) or both. The interaction also results in changes in the melt chemistry. Thus, the interaction of an eclogite-derived melt with peridotite can lead to the formation of a wide range of rocks and melts. The specific outcome of such an interaction will depend on the conditions under which it occurs (pressure, temperature, composition of the reacting melt and the host peridotite) as well as the nature of the reacting process and the of melt to rock ratio.

Many experimental studies simulated mantle metasomatism by adding $H_2O \pm CO_2$ to a single lithology (peridotite or eclogite) and exposing the system to a wide range of pressure-temperature conditions corresponding to the upper mantle [see compilation in Dvir and Kessel (2017) and Elazar et al. (2019)]. These studies are important in establishing the phase relations of the mantle in the presence of volatiles, as well as determining the P–T conditions of melt initiation, i.e., the location of the volatile-bearing solidus of each system. However, these studies cannot simulate complex metasomatic and melting reactions in a heterogeneous mantle, specifically the interaction of eclogite-derived hydrous melts and peridotitic mantle. Thus, hybrid (eclogite+peridotite) experiments are needed.

Two major capsule set-ups are employed in studying hybrid systems. One design consists of a mixture of an eclogite or an eclogite-derived melt and a peridotite powder in various

ratios in an attempt to study the equilibrium phase relationship as complete reaction was documented in such designs. In such a setup it is assumed that a reactive porous flow occurs in the mantle leading to complete infiltration of the eclogite-derived melt into the peridotite. Gao et al. (2019), Meltzer and Kessel (2020) and Saha et al. (2018) are examples of such an approach when studying the infiltration of hydrous silicate melts into a peridotite. The second design is a layered capsule. An eclogite powder or eclogite-derived melt powder is placed adjacent to a peridotite powder in a single capsule, simulating a scenario where an eclogite-derived melt is able to escape the eclogite and rise into the peridotitic mantle via a channelized flow. In such a scenario, representing a more realistic simulation of such processes, the interaction is limited to the melt–rock interface.

Most layered hybrid experimental studies were performed on anhydrous systems in order to study the evolution of ocean island basalts or melting during upwelling mantle (e.g., Borghini et al. 2022; Mallik and Dasgupta 2012; Takahashi and Gao 2015; Wang et al. 2010; Yaxley and Green 1998). Only a few studies involved volatiles in the experiments in order to better understand processes occurring at subduction zones or in the subcontinental lithospheric mantle (Carroll and Wyllie 1989; Gao et al. 2019; Gervasoni et al. 2017; Johnston and Wyllie 1989; Rapp et al. 1999; Sekine and Wyllie 1983). Most of these studies focused on the interaction of eclogite-derived hydrous melt and a fertile peridotite at 1-4 GPa, resulting in the formation of high-Mg andesite and dacite melts and enrichment of opx and grt on the expense of olivine in the metasomatized lherzolite. However, in such geological settings, an eclogite-derived hydrous melt mostly interacts with a depleted peridotite. Yet, studies on the interaction of eclogite-derived hydrous melts and harzburgite are rare.

In this contribution, we study the infiltration of a H_2O-CO_2-bearing eclogite-derived melt into a harzburgite at 4 GPa and 1200°C. The design used in this study is a layered capsule, with a diamond trap separating the two lithologies. Such a design allows us to directly analyze the liquid phase (either fluid or melt), as well as its influence on the mantle mineralogy and chemistry. Experiments were performed in a rocking multi anvil, rotated at various frequencies in order to study the progressive interaction of the eclogite-derived hydrous melt and the host harzburgite.

METHODS

Starting materials

The starting materials used in this study consist of a synthetic carbonated K-bearing basaltic powder (labeled CKB) and a synthetic depleted harzburgite (labeled DHRZ). For the basaltic composition we used an anhydrous eclogite composition similar to ATCM1 (Thomson et al. 2016). This composition was designed to represent subducted oceanic crust that has undergone dehydration reactions but no partial melting. It retains a carbonate component (~3 wt% CO_2), and elevated SiO_2 relative to other basaltic starting compositions (Fig. 1). In contrast to the low K_2O (0.06 wt%) content used by (Thomson et al. 2016), we used an elevated K_2O content (0.49 wt%), similar to KMB-7 (Schmidt and Poli 1998). The composition of the depleted harzburgite was taken from a reference natural xenolith GP8, part of a suite of ultra-depleted xenoliths from the southern Zimbabwe Craton (Smith et al. 2009). These peridotitic xenoliths are characterized by high-Mg# olivine (Mg#~0.94), as well as very low HREE abundances and low Yb/Lu ratios. They are thought to represent some of the most pristine examples of residua formed via high degree melting during craton stabilization. This

136 composition was chosen primarily because the mineralogical change due to the metasomatic
137 effect of fluid/melt liberated from the carbonate eclogite is relatively easy to assess.

138 Both starting compositions were prepared using reagent grade oxides. SiO_2, Al_2O_3, FeO,
139 MgO and Cr_2O_3 were sintered for one hour, and TiO_2, NiO and MnO were sintered for 4
140 hours, all at 800ºC. CO_2 was added to the CKB basaltic powder via $Na_2(CO)_3$, $CaCO_3$ and
141 $K_2(CO)_3$ which were sintered for 4 hours at 400ºC. The dried oxides and carbonates where
142 mixed at the appropriate proportions in both powders and ground under ethanol in an agate
143 mortar for several hours, ensuring homogenous powders. Mineral seeds were not added to the
144 starting material. The basaltic starting material was doped with 57 ppm Th. The harzburgitic
145 powder was doped with 36 ppm Cs. Both trace elements were added as internal standards for
146 quantification of LA-ICP-MS analysis of the fluid/melt phase, following the cryogenic
147 technique developed by Kessel et al. (2004). Th was added by diluting 1000 ppm HCl and
148 HNO_3 standard solutions with distilled water. Cs was added as Cs_2CO_3 dissolved in HNO_3
149 and was also diluted from a 1000 ppm standard solution using distilled water. The diluted
150 solutions were added to the staring materials and were mixed thoroughly in an agate mortar.
151 Finally, the bulk powders were doped with nano-grains of pure iridium (Ir) metal (<60
152 microns, Chempur® LTD, Poland), such that it constituted ~3% of the powder. The Ir grains
153 acted as a redox sensor for oxygen fugacity determination, following the technique developed
154 by Woodland and O'Neill (1997) and Stagno and Frost (2010). The final synthetic powders
155 were stored at 110°C to avoid absorption of atmospheric water.

156 The major element compositions of the synthetic powders were determined at the
157 geochemical lab of the Geological Survey of Israel using a Perkin Elmer Optima 3300 ICP-
158 OES against USGS standards, resulting in a confidence level of ±1% for the measurements.

159 Aliquots for the determination of Th and Cs concentrations were dissolved in $HF+HNO_3$ and
160 analyzed by ICP-MS at the Geological Survey of Israel. The compositions are presented in
161 Table 1. The bulk CO_2 content in both starting materials was determined separately, using the
162 QTS (Quartz Tube System) technique developed by Dvir et al. (2013). Two QTS
163 measurements on each powder were performed (Table 1). The eclogite powder contains ~3
164 wt% CO_2. Although no CO_2 was added to the harzburgite, it was found to contain ~0.5 wt%
165 CO_2, most probably the result of contamination during preparation.

166 **Capsule design**

167 Two control experiments were performed. One experiment contained eclogite+H_2O+CO_2
168 and the second experiment contained harzburgite+H_2O+CO_2. These experiments were run in
169 order to assess the chemistry of the fluid/melt and minerals and their proportions in each
170 system before they interact with each other. In addition, three hybrid experiments were
171 performed, containing both eclogite and harzburgite in order to assess the interaction of
172 eclogite-derived melt and harzburgite in the presence of H_2O+CO_2.

173 All experiments were conducted using Au capsules (2.0 outer diameter, 1.9 mm inner
174 diameter). First, ~1 μL H_2O was inserted at the bottom of the capsule (measured with a
175 micropipette and confirmed by weight). Then, a layer of powder (5-6 mg) was added, overlain
176 by a layer of 15-25 μm diameter synthetic diamond grains (2-3 mg). Finally, 5-6 mg of
177 powder were placed on top of the diamond layer. In the control experiment, the same powder
178 was added below and above the diamond layer. In the hybrid experiments, eclogite was
179 inserted below and harzburgite above the diamond trap. The weight ratio between the eclogite
180 and harzburgite powders in the hybrid experiments was between 0.99-1.11. In all experiments
181 the diamond trap constituted 16-20 wt% of the solid material in the capsule. Capsules were

This is the peer-reviewed, final accepted version for American Mineralogist, published by the Mineralogical Society of America.
The published version is subject to change. Cite as Authors (Year) Title. American Mineralogist, in press.
DOI: https://doi.org/10.2138/am-2022-8799. http://www.minsocam.org/

182 welded while frozen in liquid nitrogen, in order to minimize the loss of H_2O and CO_2 during
183 welding and weighed both prior to and after welding and folding. Only capsules that
184 demonstrated no significant loss of material during capsule preparation were used. Finally, the
185 capsules were squeezed to a 2-3 mm long cylinders. The experimental setup for this study is
186 given in Table 2.

187 **Experimental approach**

188 Experiments were performed at constant pressure of 4 GPa and constant temperature of
189 1200°C, conditions where the volatile-bearing eclogite is expected to partially melt while the
190 volatile-bearing harzburgite remains solid. Experiments were conducted in a 675-ton rocking
191 multi anvil press at the Institute of Earth Sciences, the Hebrew University of Jerusalem, Israel.
192 Pressure was calibrated at high temperature (1000-1200ºC) for quartz–coesite, fayalite-
193 γFe_2SiO_4, and coesite–stishovite phase transitions (Dvir et al. 2011) and is within ±0.2 GPa of
194 the quoted values. Temperature was measured using a Pt-$Pt_{10}Rh$ (type-S) thermocouple;
195 reported temperatures are not corrected for the effect of pressure on the thermocouples
196 electromotive force and are within ±2ºC from the thermocouple reading. Experiments were
197 performed using 19 mm gasket edged length MgO octahedra [fabricated from MgO-based
198 castable ceramics (Ceramacast 584)] and tungsten carbide cubes with truncation edge length
199 of 11 mm.

200 Each experiment contained two identical capsules, vertically placed one on top of the
201 other, although only one capsule in each experiment was used in this study. Each capsule was
202 loaded into a boron-nitride cylinder to minimize hydrogen loss (Truckenbrodt and Johannes
203 1999; Truckenbrodt et al. 1997). The boron nitride cylinder was placed within a 4.0 mm-outer
204 diameter stepped graphite furnace. MgO spacers and Mo caps were placed above and below

the two capsules to ensure electrical contact between the stepped furnace and the tungsten carbide cubes. The thermocouple was placed through the octahedron gaskets, as close as possible to the octahedron center between the two capsules. The temperature gradient along the capsule was not determined in these experiments. However, employing a thermal gradient of 11^{o}/mm assumed to occur in such an assembly (Konzett et al. 2011) along 2-3 mm capsules yields a temperature gradient from 1200^{o}C near the thermocouple down to 1170^{o}C at the far end of the capsules.

Previous high-pressure experiments on static multi-anvils containing fluid-bearing systems often resulted in mineralogically segregated charges, sometimes leading to unstable mineral assemblages [see discussion in Schmidt and Ulmer (2004)]. Schmidt and Ulmer (2004) demonstrated that rotation of the multi-anvil gravitationally drives the fluid phase to migrate from one end of the capsule to the other, driving reactions forward and therefore enhancing chemical equilibrium throughout the experimental charge. In all experiments in this study (except the static experiment #40), the multi-anvil was initially rotated 180^{o} constantly (each rotation takes 15 seconds) for the first hour, in order to provide equilibrium nucleation centers throughout the capsule (Melekhova et al. 2007). After 1 hour had elapsed, the rotation was set to occur at a different frequency in each experiment for the remaining duration of the experiment (Table 2). The two control experiments (#30 and #41) were rotated every 15 minutes. The hybrid experiment #35 was rotated every 15 minutes while the hybrid experiment #38 was rotated constantly. The hybrid experiment #40 remained static. The higher the frequency of rotation, the frequent migration of the fluid or melt from one end of the capsule to the other, leading to more interaction between the fluid or melt and the rock.

Increasing frequency of rotation is qualitatively taken here as an indication of increasing degree of interaction.

All experiments were run for 21-24 hours and terminated by turning off the furnace power followed by a slow unloading of pressure. Once pressure was unloaded, the assemblage was taken out and prepared for analyses.

Analytical methods

High-pressure H_2O-rich fluids and melts are rich in solute and are thus unquenchable [see discussion in Kessel et al. (2004)]. Being a homogeneous phase at run P-T, the fluid or melt undergoes exsolution during quenching, producing a mixture of H_2O-rich phase and quench precipitates. Opening the capsule in order to prepare for analyses leads to the escape of the H_2O-rich phase containing highly volatile cations (such as Na, K, Cs), leaving behind only the quench precipitates. In order to prevent such a fractionation, the fluid or melt phase composition was determined following the cryogenic technique developed by Kessel et al. (2004). In this technique, the capsule is frozen while closed and then cut vertically to expose the diamond trap. The frozen diamond trap is analyzed using a 193 nm RESOlution 193 nm ArF excimer laser system (ASI, Australia) coupled to an AnalytikJena Plasma Quant MS-Elite ICP-MS at the Institute of Earth Sciences, the Hebrew University of Jerusalem, Israel. An ablation spot diameter of 50-100 μm is used depending on the diamond trap geometry. Data was acquired in blocks of 6-14 individual analyses bracketed by 4-6 analyses of the NIST-SRM-610 standard. Dwell time was typically 40 and 60 seconds. Background was counted for 10-40 seconds and the signal for at least 40 seconds. Analyses were performed for ^{23}Na, ^{24}Mg, ^{27}Al, ^{29}Si, ^{39}K, ^{42}Ca, ^{44}Ca,^{49}Ti, ^{57}Fe, ^{53}Cr, ^{60}Ni, ^{133}Cs and ^{232}Th. In addition, ^{12}C,

249 ^{13}C, ^{197}Au and ^{193}Ir were also analyzed in order to assess the position of the laser beam. Data
250 was reduced using the SILLS program (Guillong et al. 2008).

251 The Th doped into the eclogite powder is assumed to be a highly incompatible element in
252 eclogitic systems [bulk partition coefficient of 0.002-0.02 between eclogite and H_2O-CO_2-
253 fluids or melts (Elazar et al. 2019)]. The Cs doped into the harzburgite powder is assumed to
254 be a highly incompatible element in peridotitic systems. Bulk partition coefficients for Cs are
255 in the range of 0.007-0.003 between peridotite and carbonatitic melts (Dasgupta et al. 2009)
256 and 0.002-0.01 between peridotite and hydrous fluids or melts (Kessel et al. 2015). It is,
257 therefore, assumed that all the Th and Cs in the capsule reside in the fluid or melt phase at
258 equilibrium. The known amount of Th and Cs in the fluid or melt is used to convert the
259 elemental ratios derived from the LA-ICP-MS analyses of the diamond trap to the anhydrous
260 composition of the fluid or melt, following the technique developed in Kessel et al. (2004).

261 Following the LA-ICP-MS analysis of the total dissolved solids in the fluid/melt phase,
262 the capsule was defrosted and prepared for analysis of the minerals. Capsules were polished
263 using an ATM© Sapphire 520 grinder and polisher using anhydrous silicon carbide (SiC) and
264 polycrystalline diamond pastes in order to prevent loss of volatile phases. Phase identification,
265 composition and textural relations were established using a Jeol-JXA-8230 electron probe
266 micro analyzer (EPMA) at the Hebrew University of Jerusalem, Israel. All measurements
267 were preformed using an accelerating voltage of 15 keV and beam current of 15 nA, against
268 silicate and oxide standards. Chemical characterization of the phases was performed with a
269 minimum duration of 30 seconds for the signal and 10 seconds for the background. All phases
270 were analyzed for Si, Ti, Al, Fe, Mg, Ca, Na, K, and Cr. Au capsule walls were also analyzed
271 for elemental contamination.

No hydrous or carbonated crystalline phases were observed in the experiments. Thus, all the H_2O and CO_2 inserted into the capsule were assumed to reside in the fluid or melt phase. The masses of CO_2 and H_2O are then combined with the mass of all cations in the fluid or melt to derive the complete major element composition of the fluid or melt phase in each capsule.

Phase abundance calculations

The abundance of each phase in each experiment was determined using Monte Carlo calculations based on major element compositions of all minerals, fluid or melt composition and the composition of the bulk material inserted into the capsule. The anhydrous algorithm used a non-weighted least square fit, performing 10,000 calculation runs, by modifying the compositions within the error range given by 1 σ. The 10,000 results were collected and the average and 1 σ of the phase abundance were calculated.

Oxygen fugacity analyses

Oxygen fugacity in these experiments was determined by analyzing the Fe content in Ir grains throughout the capsule. The Ir grains act as fO_2 sensors, following the method of Stagno and Frost (2010). In this approach, Fe in Ir grains is equilibrated with Fe in silicates and the $\log fO_2$ can be calculated by employing activity-composition models for the various phases as well as their ΔG^o (the free energy of the pure end members).

In each experiment, 11-14 Ir grains, located along the capsule from the edge of the diamond trap to the end of the peridotite layer were analyzed via EPMA. Signal time was set to 35 seconds and background time was set to 15 seconds. The concentrations of Si, Mg, Ca, Ti and Cr were monitored in these grains in order to avoid silicate contamination. Only grains

with no apparent contamination (i.e., Si, Mg, Ca and Ti concentrations below 0.2 wt%) were chosen for oxygen fugacity calculations.

RESULTS

The harzburgite+H_2O+CO_2 control experiment (#30) contains mostly olivine (ol) and orthopyroxene (opx) with a small amount of garnet (Fig. 2a). No clinopyroxene (cpx) is observed in the harzburgite. All phases are homogeneously distributed in both sides of the diamond trap. Quench precipitates are trapped in between the diamond grains. The eclogite+H_2O+CO_2 control experiment (#41) is composed of mostly quench glass in and outside the diamond trap (Fig. 2b). Garnet crystals appear around the diamond trap and at the top of the capsule.

In all three hybrid experiments, the interaction of eclogite and harzburgite resulted in stratified capsules (Fig. 3a-c) containing a reaction layer between the eclogite and the peridotite. In the static experiment (#40), the sequence from bottom up includes a quench layer composed of small quench precipitates, a layer of eclogitic garnet, the diamond trap, a thin reaction layer containing large grains of garnet and opx, overlain by a peridotitic layer composed of olivine, opx, cpx and small amount of garnet grains, mostly close to the reaction layer. In the two rocking experiments (#35, rocked every 15 minutes and #38, rocked every 15 seconds), quench precipitates appear at the bottom of the capsule, overlain by the diamond trap. Above the diamond trap, a thick reaction layer containing garnet+opx±cpx has formed that is overlain by a peridotite layer composed of olivine, opx, cpx and some garnet. Although cpx was not stable in any of the control experiments (harzburgite+H_2O+CO_2 and eclogite+H_2O+CO_2 systems), it appears in all rocking experiments as part of the peridotite

316 layer. In all hybrid experiments, cracks are seen in the reaction layers, perpendicular to the
317 layer, from the eclogite to the peridotite.

318 In each experiment, 4-37 individual grains of each mineral phase were analyzed
319 throughout the capsule. Care was taken to exclusively measure the rim compositions (the
320 outer 10 microns), which is in equilibrium with their surrounding phases. Mineral
321 compositions are provided in Tables 3-6 and Figs. 4-6. Uncertainties reported throughout this
322 study are one standard deviation of n analyses (1σ).

323 Quench precipitates are present in the diamond trap in all experiments, indicating the
324 existence of a fluid or melt phase in equilibrium with the surrounding rocks. In each
325 experiment, 5-14 analyses were performed along the diamond trap in order to derive the fluid
326 or melt compositions. The composition of the liquid phase in the eclogite control experiment
327 was calculated based on the Th doped into the starting material, acting as internal standards in
328 the LA-ICP-MS analyses. The composition of the liquid phase in the harzburgite control
329 experiment was calculated based on the Cs doped into the starting material. In all hybrid
330 experiment, the composition of the liquid phase was calculated once based on Th and once
331 based on Cs. The liquid phase composition calculated by both methods (via Th or Cs as
332 internal standard) are similar within uncertainties (Table S1 and Figs. S1-2 in supplement),
333 supporting our assumption of their incompatibility in such systems. The fluid or melt phase
334 compositions presented in Table 7 and Fig. 7 were derived from Th as an internal standard,
335 except in the harzburgite control experiment, where the data was derived from Cs.

336 **Harzburgite+H_2O+CO_2 control experiment**

337 The mineral assemblage in the harzburgite control experiment (#30) consists of ol, opx
338 and garnet. *Olivine* is the main phase in the harzburgite. It is forsteritic in nature, with Mg#

[Mg/(Mg +Fe) in molar unit] of 0.94 (Fig. 4), slightly higher than the #Mg of the initial GP8 harzburgite composition (Table 1). It appears subhedral with size ranging from 10-50 μm throughout the capsule to 50-100 μm near the diamond trap. *Orthopyroxene* is enstatite-rich with Mg# of 0.95 (Fig. 4), containing 0.2 wt% CaO and 1.2 wt% Al_2O_3. The opx appears subhedral, 20-70 μm in size. *Garnet* is Cr-rich pyrope ($Pyrop_{0.73}Alm_{0.10}Gros_{0.05}$), containing 3.2 wt% Cr_2O_3 and 2.3 wt% CaO (Figs. 5-6), falling within the harzburgititc field (Grütter et al. 2006).

The liquid in equilibrium with the harzburgite at 4 GPa and 1200°C contains 62.6 wt% H_2O and 2.9 wt% CO_2 (Fig. 7), indicating an aqueous fluid nature. The fluid phase is metaluminous [molar Al/(2Ca+Na+K)< 1] in character, containing 42.2 wt% SiO_2 and 23.2 wt% MgO.

Eclogite+H_2O+CO_2 control experiment

The eclogite+H_2O+CO_2 control experiment (#41) is comprised solely of garnet in equilibrium with a liquid phase (Fig. 2b). Garnet appears euhedral to subhedral, located mostly above the diamond trap. The garnet grains are 10-100 μm in size. They are characterized by Mg# of 0.62 and contain 0.01 wt% Cr_2O_3 and 8.2 wt% CaO, falling within the eclogitic field (Fig. 6). The garnet composition is $Pyrop_{0.41}Alm_{0.25}Gros_{0.19}$ (Fig. 5).

The liquid phase in this experiment contains 6.8 wt% H_2O, 2.3 wt% CO_2, 50 wt% SiO_2 and 4.5 wt% Na_2O+K_2O, thus identified as a metaluminous andesitic melt. This melt is assumed to infiltrate and react with the harzburgite in the hybrid experiments.

359 **Hybrid eclogite+peridotite experiments**

360 Three hybrid experiments were performed. All experiments initially contained similar
361 amounts of eclogite and harzburgite powder, with a diamond trap placed in between the two
362 layers (Table 2, Fig. 3). Thus, all three capsules are considered to contain similar bulk
363 compositions. However, each experiment was rotated at a different frequency (static, every 15
364 minutes, every 15 seconds).

365 In the static hybrid experiment (#40), a layer of eclogitic garnets appears below the
366 diamond trap. Their composition is similar to that in the eclogite+H_2O+CO_2 control
367 experiment, with only slightly higher CaO content and higher Mg# (Figs. 5, 6). Above the
368 diamond trap, a thin reaction layer was formed composed of garnet grains. They are
369 intermediate in composition between the eclogitic and harzburgitic garnets in the control
370 experiments, with composition of $Pyrop_{0.65}Alm_{0.16}Gros_{0.12}$, Cr_2O_3 content of 0.7 wt% and
371 CaO of 4.8 wt%. Above the reaction layer, a peridotite containing olivine, opx and cpx is
372 stable. The olivine appears as small subheadral grains, forsteritic in composition and the opx
373 is enstatitic, both are characterized by Mg# of 0.93, only slightly lower than in the
374 harzburgite+H_2O+CO_2 control experiment (Fig. 4). The cpx grains are Mg-rich augite,
375 characterized by Mg# of 0.94; CaO of 20.0 wt%, Al_2O_3 of 1.4 wt% and Na_2O of 2.2 wt%.

376 In both rotating experiments (#35 and #38), no garnet is present in the eclogite side of the
377 experiment. The diamond trap was displaced to the bottom of the capsule and a thick reaction
378 layer was formed above the diamond layer, containing garnet and opx. The garnet grains close
379 to the diamond trap contain 6-7 wt% CaO and ~0.2 wt% Cr_2O_3, falling in the eclogitic garnet
380 field. They are intermediate in composition between the eclogitic garnet and the peridotitic
381 garnet in the control experiments ($Pyrop_{0.65}Alm_{0.16\text{-}0.17}Gros_{0.17\text{-}0.18}$). The garnet grains in the

382 far side of the reaction layer are more peridotitic in nature. They are slightly enriched in
383 pyrope and depleted in almandine than the eclogitic garnets in these experiments ($Pyrop_{0.69-0.71}Alm_{0.12-0.18}Gros_{0.13-0.17}$), and contain 6-7 wt% CaO and 3-5 wt% Cr_2O_3. The olivine in the
385 peridotitic layer is subhedral, 10-50 μm in size. It is slightly less forsteritic than in the
386 harzburgite control experiment and the static experiment (Mg# of 0.92). The opx in these
387 experiments is also slightly less enstatitic with Mg# of 0.93. The jadeite component in the cpx
388 is 0.6-0.8.

389 In all hybrid experiments, a melt phase is trapped in between the diamonds. The melt in
390 the static experiment is metaluminous, containing 50.0 wt% SiO_2, 15.5 wt% H_2O, 2.8 wt%
391 CO_2 and 4.9 wt% Na_2O+K_2O (Fig. 7). The melt in both rocking experiments is peralkaline
392 (molar $(Na_2O/Al_2O_3 >1)$, containing 28-34 wt% SiO_2, 20-25 wt% H_2O, 5 wt% CO_2 and 6-7
393 wt% Na_2O+K_2O. While the melt phase in the static experiment is close in composition to the
394 melt in equilibrium with eclogite only, the composition of the melt in the rocking experiments
395 is an average between the fluid in equilibrium with harzburgite and the melt in equilibrium
396 with eclogite (Fig. 7).

397 **Phase abundance**

398 The phase abundance in each experiment is given in Table 8 and shown in Fig. 8. The
399 eclogite+H_2O+CO_2 system in this study is super-solidus, consisting of ~24% garnet and 76%
400 melt while the harzburgite+H_2O+CO_2 system is sub-solidus, containing 58% olivine, 25%
401 opx, 1% garnet and 15% fluid. In the static hybrid experiment, the amount of eclogitic garnet
402 in the bulk system is 42%. Its amount decreases to 27-28% in both rocking hybrid
403 experiments. The peridotitic olivine in the static experiment constitutes 16% of the bulk
404 system. Its abundance is reduced to 8-11% with increasing frequency of rotation. The

peridotitic opx in the static experiment constitutes 17% of the system, increasing to 26-31% as rotation is set. The peridotitic cpx, absent in the original harzburgite, is formed during the interaction between the eclogite-derived melt and harzburgite. It constitutes 4% of the bulk system in the static experiment, increasing to 8-13% in the rotating experiments. Minor amount (~3%) of peridotitic garnet is also present in all hybrid experiments. The amount of melt in the system increases from 19 to 25% with increasing rotation frequency.

Oxygen fugacity

Following Stagno and Frost (2010), the equilibrium between Ir grains, olivine and opx fixes the logfO_2 of the assembly. Only garnet and melt are stable in the eclogite+H_2O+CO_2 control experiment, thus no fO_2 calculations are available for this experiment.

Olivine, opx and Ir grains are present in the harzburgite+H_2O+CO_2 control experiment as well as in all three hybrid experiments. The compositions of olivine and opx in each of these experiments are homogeneous throughout the capsule (Fig. 4). The Fe content in Ir grains was analyzed in each capsule from the edge of the diamond trap to the end of the peridotite layer and the local logfO_2 was calculated (Fig. 9). The mole fraction of Fe in the Ir grains (X_{Fe}^{Ir}) in the harzburgite+H_2O+CO_2 control experiment is 0.02-0.10, with no apparent dependence on the location in the capsule. The logfO_2 registered by the Ir grains ranges between -7.7 to -6.1 (1.89±0.40 log units below the QFM buffer), considered constant within the uncertainties of the method. The X_{Fe}^{Ir} in the static experiment (#40) and the hybrid experiment rotated every 15 minutes (#35) varies systematically from 0.21 in the edge of the reaction layer to 0.31 in the far end of the peridotite layer, corresponding to a decrease in log fO_2 from -8.7 to -9.5 (3.4 to 4.2 log units below QFM, respectively). A similar trend is observed in the hybrid experiment rotated every 15 seconds (#38), albeit at slightly higher values. The logfO_2

428 decreases from 2.0 log units below QFM to 2.9 log units below QFM. All logfO_2 values
429 recorded in these experiments are below EMOD (enstatite-magnesite-olivine-diamond)
430 reference curve, which is the limiting reaction for the diamond stability field [taken from
431 Eggler and Baker (1982)].

432 ## DISCUSSION

433 ### Approach to equilibrium

434 The initial synthetic powders in all capsules were converted to high-pressure and high-
435 temperature mineral assemblies. Phases are homogeneously distributed in each layer and no
436 major internal zoning is observed in the minerals. The amount of Fe diffused into the Au
437 capsule is less than 0.2 wt% close to the experimental charge, indicating no significant Fe loss
438 to the capsule. Close to the edge of the Au capsule, Fe content is below detection limit (0.02
439 wt%). All these observations suggest that all capsules, including the hybrid experiments,
440 demonstrate an equilibrium set up. In addition, the chemical compositions of opx and cpx in
441 the hybrid experiments indicate an equilibrium temperature of 1180-1260^{o}C (Table 2), based
442 on the Mg-Fe exchange between the two minerals (Putirka 2008). These temperatures are
443 within the range of temperatures experienced by the capsules.

444 ### Mineral and melt compositions

445 In both eclogite+H_2O (Kessel et al. 2005) and eclogite+H_2O+CO_2 (Elazar et al. 2019)
446 systems, the second critical endpoint was found to be between 5 and 6 GPa, indicating the
447 existence of a solidus at 4 GPa. Thus, the eclogite+H_2O+CO_2 control experiment in this study
448 (4 GPa and 1200^{o}C) is assumed to be at super-solidus conditions. The capsule is composed of
449 only garnet in equilibrium with melt. Mass balance calculations indicate that 76% melt is
450 present in the capsule (Table 8). Elazar et al. (2019) studied a similar eclogite+H_2O+CO_2

system. Their eclogite, similar to SCLM1 (Dasgupta et al. 2004), is slightly depleted in SiO_2 and Al_2O_3 relative to the eclogite in this study (43 and 11 comparted to 51 and 15 wt%, respectively, Fig. 1). While a similar H_2O content was added in both Elazar et al. (2019) and this study (9 and 10 wt%, respectively), higher CO_2 of 10 wt% was added in Elazar et al. (2019) compared with only 3 wt% in this study. As a consequence, at 4 GPa, the solidus in Elazar et al. (2019) was found to be between 1000 and 1100°C. At 1200°C, the system in Elazar et al. (2019) is composed of garnet, cpx, rutile, magnesite and kyanite, in equilibrium with 70% melt containing 13 wt% H_2O and 15 wt% CO_2. In the current study at 1200°C, higher amount of melt was found, containing lower amounts of H_2O (7 wt%) and CO_2 (2 wt%) indicating a lower solidus temperature than in Elazar et al. (2019). The melt in equilibrium with eclogite in this study is metaluminous, similar to the near-solidus melt in Elazar et al. (2019).

Most previous studies on peridotite+H_2O+CO_2 systems focused on lherzolitic composition [Dvir and Kessel (2017) and references therein]. All the studies mentioned in Dvir and Kessel (2017) determined the location of the solidus at 4 GPa, albeit its location varies due to differences in bulk composition. Nevertheless, these studies demonstrate that the system is below its second critical endpoint. Studies on harzburgite+H_2O+CO_2 are limited so no direct comparison to the current study is available. The harzburgite+H_2O+CO_2 control experiment in this study is sub-solidus, containing a fluid phase in equilibrium with 58% olivine, 25% opx and 1% garnet. Wyllie (1987) has determined the solidus of such a system to be above 1400°C at 4 GPa, in agreement with our findings of the system to be sub-solidus at 1200°C. A metaluminous fluid is in equilibrium with the harzburgite at these conditions.

All three hybrid experiments were performed containing eclogite and harzburgite, juxtaposed one above the other, in the presence of H_2O and CO_2. The H_2O-CO_2-bearing melt formed in the eclogite control experiment is assumed to interact with the harzburgite in the hybrid experiments. In all scenarios examined in this study, a H_2O-CO_2-bearing melt was formed. Cracks, seen in all reaction layers in the hybrid experiments crossing from the eclogite to the peridotite (Fig. 3), allow the eclogite-derived hydrous melt to move through the reaction layer into the peridotite layer (i.e., allowing channelized flow) promoting melt-rock interaction. The appearance of cpx in the peridotite layer indicates that some interaction occurs also at the far end of the capsule as well. However, the degree of interaction, shown both by changes in mineral and melt compositions as well as the amount of newly formed minerals, is a function of frequency of rotation, thus degree of interaction.

The static interaction between eclogite and harzburgite resulted in the formation of a metaluminous melt, characterized by only slightly higher Mg# and lower Ca# [Ca/(Ca+Mg+Fe)] than the melt in equilibrium with only eclogite (Fig. 7e). Rotation of the multi-anvil led to the formation of a melt intermediate in composition between the fluid in equilibrium with harzburgite and the melt in equilibrium with eclogite in the control experiments. Increasing frequency of rotation lowered the SiO_2 and Al_2O_3 contents of the melt while increased the MgO, H_2O and CO_2 and alkali contents towards the composition of the fluid in the harzburgite control experiment. These changes in chemistry lead to a change in character from metaluminous to peralkaline melt. The more frequent the rotation is, the more peralkaline the melt is (Fig. 8).

The initial harzburgite constitutes ol, opx and garnet. In all hybrid experiments the peridotite contains a similar mineral assemblage of ol, opx, cpx, grt. However, the

This is the peer-reviewed, final accepted version for American Mineralogist, published by the Mineralogical Society of America.
The published version is subject to change. Cite as Authors (Year) Title. American Mineralogist, in press.
DOI: https://doi.org/10.2138/am-2022-8799. http://www.minsocam.org/

compositions of the minerals change with increasing interaction between the harzburgite and the eclogite-derived hydrous melt (Figs. 4-6). In the static experiment, the eclogitic garnet is similar in composition to the garnet in the eclogite control experiment. The peridotitic garnet is intermediate in composition between the eclogitic and peridotitic garnets in the control experiments. The Mg# of the peridotitic ol and opx is slightly lower than that of the harzburgite control experiment. More pronounced changes in mineral composition are observed in the rotation experiment. Both the eclogitic garnets and the peridotitic garnets approach each other in composition, both in Mg# as well as in CaO and Cr_2O_3 contents. The Mg# values of ol and opx are significantly lower than the values in the harzburgite control experiment. Clinopyroxene, absent in both the initial harzburgite and eclogite, appear in all hybrid experiments. The Mg# of the cpx in the hybrid experiments is also lower and the jadeite component is higher compared to the static experiment.

Increasing interaction between the eclogite and the harzburgite at a constant eclogite:harzburgite ratio at a given P-T conditions led to increasing change in mineral chemistry towards an intermediate composition between the eclogite and harzburgite. However, the enhanced interaction did not cause the disappearance of the reaction layer between the two lithologies. Rather, increasing interaction led to increasing thickness of the reaction layer. This observation is in accord with Bulatov et al. (2014) who demonstrated that a reaction layer remains even after long duration of metasomatism, preventing complete equilibration.

Oxygen fugacity during metasomatic reaction

The oxygen fugacity registered by the Ir-Fe grains in the harzburgite control experiment is 2.0±0.2 log units below QFM, ranging from 1.6 to 2.2 log units below QFM buffer (Fig. 9),

519 ~0.6 log units below the enstatite-magnesite-olivine-diamond (EMOD) buffer. The logfO_2
520 values are identical within uncertainties throughout the capsule, regardless of the location of
521 the Ir grain, indicating a high degree of equilibrium in this experiment.

522 In all hybrid experiments, the logfO_2 is more reducing than in the harzburgite control
523 experiment and exhibit a gradient from relatively more oxidizing conditions near the reaction
524 layer, towards more reducing conditions further away into the peridotite layer. In both the
525 static and the slow rotating experiment, logfO_2 changes systematically from QFM-3.4 to
526 QFM-4.2. In the fast-rotated experiment (#38), the logfO_2 exhibits similar gradient, albeit the
527 fO_2 is ~1 log unit more oxidizing, from QFM-2.3 close to the reaction layer down to QFM-2.9
528 in the far end of the peridotite. The logfO_2 close to the reaction layer is similar to the logfO_2 in
529 the harzburgite control experiment.

530 The bulk composition in the harzburgite control experiment contains ~10 wt% H_2O and
531 0.4 wt% CO_2. The fluid in equilibrium with harzburgite contains ~63 wt% H_2O. Water acts as
532 an efficient oxidizing agent. Kelley and Cottrell (2009) showed that the H_2O concentrations in
533 the fluid or melt and the oxidation state of Fe linearly correlate. High H_2O content in the fluid
534 in this experiment suggests high $Fe^{3+}/\Sigma Fe$ ratio, imposing relatively oxidizing conditions.
535 Since the experiment was constantly rotated and the fluid freely traversed throughout the
536 capsule, a homogeneous logfO_2 values are registered in the harzburgite on both sides of the
537 diamond trap.

538 In the hybrid experiments, eclogite and harzburgite were mixed in equal proportions. The
539 bulk H_2O in the capsule is 7-8 wt% H_2O and 1.6 wt% CO_2. The melt in all three experiments
540 contains 15-25 wt% H_2O and 2-5 wt% CO_2, lowering the activity of H_2O in the melt. Lower
541 H_2O content correlates with lower $Fe^{3+}/\Sigma Fe$ ratio, suggesting a more reducing conditions in

This is the peer-reviewed, final accepted version for American Mineralogist, published by the Mineralogical Society of America.
The published version is subject to change. Cite as Authors (Year) Title. American Mineralogist, in press.
DOI: https://doi.org/10.2138/am-2022-8799. http://www.minsocam.org/

542 these capsules. The melts in these experiments originated in the eclogite layer, travelled and
543 filled the diamond trap and interacted with the harzburgite, forming a reaction zone. The
544 logfO_2 values registered at the edge of the reaction zones reflect the more reducing conditions
545 in these melts compared to the harzburgite control experiment. The decrease in logfO_2 from
546 the edge of the reaction zone into the peridotite suggests that the reaction zones act as partial
547 barberries for the melt to travel through the peridotite. The logfO_2 profile of experiment #38
548 (rotation every 15 seconds) is at higher values than of experiments #40 and #35 (static and
549 rotation every 15 minutes). This is probably due to the fast rotation in this experiment,
550 allowing better interaction of the melt with the peridotitic layer.

551 **Metasomatic interaction of eclogite-derived hydrous melt and harzburgite**

552 The phase abundance in each experiment (Table 8) allows us to quantify the changes
553 occurring as a function of increasing interaction between the eclogite and harzburgite due to
554 the rotation of the multi-anvil (compared to the static experiment) at 4 GPa and 1200^{o}C. The
555 effect of increasing interaction is shown in Fig. 8 and can be summarized in the following
556 reaction:

557 $$0.7\ ol + 2.4\ grt_{ecl} = 1.3\ opx + 0.7\ cpx + 0.2\ grt_{perd} + 1.0\ melt \quad (1)$$

558 Reaction (1) demonstrates the metasomatizing effect of the eclogite-derived hydrous melt
559 on the harzburgite, by increasing the mode of the peridotitic opx, cpx and garnet (mostly as a
560 reaction layer between the eclogite and harzburgite) on the expense of peridotitic olivine and
561 the eclogitic garnet. Slight increase in melt fraction occurs with increasing interaction.

562 The formation of a reaction layer with sharp boundaries during the interaction of hydrous
563 eclogite-derived melt with harzburgite in this study is in accord with previous studies.

However, the minerals composing the reaction layer vary in previous studies as a function of the eclogite and peridotite compositions and the melt/peridotite ratio. (Sekine and Wyllie, 1983), (Carroll and Wyllie, 1989) and (Johnston and Wyllie, 1989) performed experiments containing water-saturated silicate melt and peridotite at 1.5-3 GPa and 850-1150^{o}C and observed opx+cpx±grt±phlogopite reaction layers. (Kelemen et al., 1990) conducted experiments containing olivine-tholeiite melt and hydrous harzburgite at 0.5 GPa and 1050-1150^{o}C and identified an opx-rich reaction layer. (Rapp et al., 1999) performed experiments containing amphibolitized basalt and harzburgite at 3.8 GPa and 1100-1150^{o}C. The reaction layer in this study consisted of grt±opx. They demonstrated that opx is formed when an eclogite-derived melt infiltrates a depleted peridotite, while cpx is formed when the melt infiltrates a fertile peridotite. In this study, it is demonstrated that increasing reaction between the eclogite-derived hydrous melt with harzburgite at a constant pressure and temperature increases the reaction layer, i.e., increases the amount of opx and cpx formed on the expense of peridotitic olivine and eclogitic garnet. The fraction of melt increases as well.

Implications to interaction of eclogite-derived melts and harzburgite

The eclogite-harzburgite interaction experiments documented here may provide further understanding of the chemical and modal heterogeneity in the mantle and the wide range of melts. This interaction can occur in subduction zones where eclogite-derived hydrous melts infiltrate into harzburgitic mantle adjacent to the subducting slab or in sub continental lithospheric mantle. Static interaction between eclogite and harzburgite simulates a scenario where the eclogite-derived melt rises through the harzburgitic peridotite with little time to interact with the harzburgitic walls. This experiment demonstrates that little interaction occurs. The composition of the melt is similar to the melt derived from melting of volatile-bearing

587 eclogite, a metaluminous andesitic melts. In such a setting, the eclogite-derived hydrous melt is
588 only slightly reactive towards the surrounding peridotite. Close to the boundary between the
589 eclogite and harzburgite, the eclogite-derived hydrous melt consumes the harzburgitic olivine
590 while the mode of opx increases and new cpx grains are formed in a narrow boundary layer. The
591 addition of cpx, homogeneously distributed throughout the peridotitic layer, transforms the
592 harzburgitic peridotite to lherzolitic peridotite. This re-fertilization of the mantle by metasomatic
593 melt is called stealth metasomatism (O'Reilly and Griffin 2013). New phases are formed while
594 slight changes in the composition of the pre-existing minerals occur. Grütter and Menzies (2017)
595 suggested that at low metasome/rock ratio, interaction between Al_2O_3-bearing fluid with an Al-
596 depleted harzbguite can lead to the formation of new garnet growth. This metasomatic garnet
597 growth can also be manifested as core-to-rim zonation vectors in CaO-Cr_2O_3 space, which reflect
598 changing garnet Cr/(Cr+Al) in response to changing bulk Cr/(Cr+Al). The compositional vectors
599 for the large dataset of garnets form the Newlands kimberlite (Fig. 1 of Grütter et al. 2017) are
600 similar to that found in the equilibrium assemblage in our reaction experiments (Fig. 6),
601 suggesting that an eclogite-derived fluids or melts can promote such reactions.

602 Rotation of hybrid eclogite-peridotite system simulates enhanced interaction between the
603 eclogite-derived hydrous melt and the surrounding harzburgite. Increasing interaction
604 between the eclogite-derived hydrous melt and the harzburgite leads to increasing proportion
605 of the peridotitic olivine that is consumed while the proportions of opx and cpx increase,
606 resulting in a thicker reaction zone. The mineral compositions trend towards homogeneity
607 throughout the mixing zone. The reactive melt becomes peralkaline, intermediate in
608 composition between the H_2O-CO_2 eclogitic melt and H_2O-CO_2-peridotitic fluid.

609 The interaction between eclogite-derived hydrous melt and harzburgite play an important
610 role in the mineralogical and chemical modification of the subcontinental mantle lithosphere
611 and the mantle wedge, as well as the formation of a wide range of magmas. The above
612 experiments suggest that the degree of interaction between the slab-derived melts with the
613 hosting peridotitic rocks is an important parameter, together with the initial eclogite and
614 peridotite compositions, in forming the wide range of melt compositions, from metaluminus
615 to peralkaline. The degree of interaction also influences the mineral chemistry in the residual
616 metasomatized mantle and the width of the reaction layer between the two lithologies.

617 ## ACKNOWLEDGEMENT

618 This research was supported by Israel Science Foundation grants (167/14; 760/18). We
619 thank Omri Dvir for his help with the LA-ICP-MS analyses and Yael Kempe for her help with
620 the EPMA analyses. Constructive reviews by Veronique Le Roux and an anonymous reviewer
621 helped to improve this manuscript and are greatly appreciated.

622 ## REFERENCES CITED

623 Allègre, C.J., and Turcotte, D.L. (1986) Implications of a two-component marble-cake mantle.
624 Nature, 323(6084), 123-127.
625 Atherton, M.P., and Tarney, J. (1979) Origin of Granite Batholiths: Geochemical Evidence:
626 Based on a Meeting of the Geochemistry Group of the Mineralogical Society. Springer.
627 Bell, D.R., Grégoire, M., Grove, T.L., Chatterjee, N., Carlson, R.W., and Buseck, P.R. (2005)
628 Silica and volatile-element metasomatism of Archean mantle: a xenolith-scale example
629 from the Kaapvaal Craton. Contributions to Mineralogy and Petrology, 150, 251-267.
630 Borghini, G., P, F., and E, P. (2022) Melt–rock interactions in a veined mantle:pyroxenite–
631 peridotite reaction experiments at 2 GPa. 34, 109-129.
632 Boyd, F. (1989) Compositional distinction between oceanic and cratonic lithosphere. Earth and
633 Planetary Science Letters, 96(1-2), 15-26.
634 Bulatov, V.K., Brey, G.P., Girnis, A.V., Gerdes, A., and Höfer, H.E. (2014) Carbonated
635 sediment–peridotite interaction and melting at 7.5–12GPa. Lithos, 200, 368-385.
636 Carroll, M.R., and Wyllie, P.J. (1989) Experimental phase relations in the system tonalite-
637 peridotite-H2O at 15 kb; implications for assimilation and differentiation processes near
638 the crust-mantle boundary. Journal of Petrology, 30, 1351-1382.

639 Dasgupta, R., Hirschmann, M.M., and Dellas, N. (2005) The effect of bulk composition on the
640 solidus of carbonated eclogite from partial melting experiments at 3 GPa. Contributions
641 to Mineralogy and Petrology, 149(3), 288-305.
642 Dasgupta, R., Hirschmann, M.M., McDonough, W.F., Spiegelman, M., and Withers, A.C. (2009)
643 Trace element partitioning between garnet lherzolite and carbonatite at 6.6 and 8.6 GPa
644 with applications to the geochemistry of the mantle and of mantle-derived melts.
645 Chemical Geology, 262(1-2), 57-77.
646 Dasgupta, R., Hirschmann, M.M., and Withers, A.C. (2004) Deep global cycling of carbon
647 constrained by the solidus of anhydrous, carbonated eclogite under upper mantle
648 conditions. Earth and Planetary Science Letters, 227, 73-85.
649 DePaolo, D.J. (1981) Trace element and isotopic effects of combined wallrock assimilation and
650 fractional crystallization. Earth and planetary science letters, 53, 189-202.
651 Dvir, O., Angert, A., and Kessel, R. (2013) Determining the composition of C–H–O liquids
652 following high-pressure and high-temperature diamond-trap experiments. Contributions
653 to Mineralogy and Petrology, 165, 593-599.
654 Dvir, O., and Kessel, R. (2017) The effect of CO_2 on the water-saturated solidus of K-poor
655 peridotite between 4 and 6 GPa. Geochimica et Cosmochimica Acta, 206, 184-200.
656 Dvir, O., Pettke, T., Fumagalli, P., and Kessel, R. (2011) Fluids in the peridotite–water system
657 up to 6 GPa and 800°C: new experimental constrains on dehydration reactions.
658 Contributions to Mineralogy and Petrology, 161, 829-844.
659 Eggler, D.H. (1978) Stability of dolomite in a hydrous mantle, with implications for the mantle
660 solidus. Geology, 6(7).
661 Eggler, D.H. and Baker, D. R. (1982) Reduced volatiles in the system C-O-H: implications to
662 mantle melting, fluid formation and diamond genesis. Advances in Earth and Planetary
663 Sciences, 12, 237-250.
664 Elazar, O., Frost, D., Navon, O., and Kessel, R. (2019) Melting of H_2O and CO_2-bearing eclogite
665 at 4–6 GPa and 900–1200 °C: Implications for the generation of diamond-forming fluids.
666 Geochimica et Cosmochimica Acta, 255, 69-87.
667 Gao, M., Xu, H., Zhang, J., and Foley, S.F. (2019) Experimental interaction of granitic melt and
668 peridotite at 1.5 GPa: Implications for the origin of post-collisional K-rich magmatism in
669 continental subduction zones. Lithos, 350-351.
670 Gervasoni, F., Klemme, S., Rohrbach, A., Grützner, T., and Berndt, J. (2017) Experimental
671 constraints on mantle metasomatism caused by silicate and carbonate melts. Lithos, 282-
672 283, 173-186.
673 Grütter, H., Latti, D., and Menzies, A. (2006) Cr-saturation arrays in concentrate garnet
674 compositions from Kimberlite and their use in mantle barometry. Journal of Petrology,
675 47, 801-820.
676 Grütter, H.S., and Menzies, A.H. (2017) Discrete Ti-Al±Ca metasomatism at ~53 kbar in
677 chromite-garnet peridotites from Newlands kimberlite, South Africa. 11th International
678 Kimberlite Conference, 11IKC- 4500.

679 Guillong, M., Meier, D.L., Allan, M.M., Heinrich, C.A., and Yardley, B.W. (2008) Appendix
680 A6: SILLS: A MATLAB-based program for the reduction of laser ablation ICP-MS data
681 of homogeneous materials and inclusions. Mineralogical Association of Canada Short
682 Course, 40, 328-333.
683 Helffrich, G.R., and Wood, B.J. (2001) The Earth's mantle. Nature, 412, 501-507.

Hildreth, W. (1981) Gradients in silicic magma chambers: implications for lithospheric magmatism. Journal of Geophysical Research: Solid Earth, 86, 10153-10192.

Hofmann, A.W. (1988) Chemical differentiation of the Earth: the relationship between mantle, continental crust, and oceanic crust. Earth and Planetary Science Letters, 90, 297-314.

Hofmann, A.W. (1997) Mantle geochemistry: the message from oceanic volcanism. Nature, 385(6613), 219-229.

Jackson, M.G., and Dasgupta, R. (2008) Compositions of HIMU, EM1, and EM2 from global trends between radiogenic isotopes and major elements in ocean island basalts. Earth and Planetary Science Letters, 276, 175-186.

Johnston, A.D., and Wyllie, P.J. (1989) The system tonalite-peridotite-H_2O at 30 kbar, with applications to hybridization in subduction zone magmatism. Contributions to Mineralogy and Petrology, 102, 257-264.

Kay, R.W. (1980) Volcanic arc magmas: implications of a melting-mixing model for element recycling in the crust-upper mantle system. The Journal of Geology, 88, 497-522.

Kelemen, P.B., Dick, H.J., and Quick, J.E. (1992) Formation of harzburgite by pervasive melt/rock reaction in the upper mantle. Nature, 358(6388), 635-641.

Kelemen, P.B., Hart, S.R., and Bernstein, S. (1998) Silica enrichment in the continental upper mantle via melt/rock reaction. Earth and Planetary Science Letters, 164(1-2), 387-406.

Kelemen, P.B., Joyce, D.B., Webster, J.D., and Holloway, J.R. (1990) Reaction between ultramafic rock and fractionating basaltic magma I. Phase relations, the origin of calc-alkaline magma series, and the formation of discordant dunite. Journal of petrology, 31, 51-98.

Kessel, R., Pettke, T., Fumagalli, P. (2015) Melting of metasomatized peridotite at 4-6 GPa and up to 1200^{o}C: an experimental approach. Contributions to Mineralogy and Petrology, 169, 37-56.

Kessel, R., Ulmer, P., Pettke, T., Schmidt, M.W. and Thompson, A.B. (2004) A novel approach to determine high-pressure high-temperature fluid and melt compositions using diamond-trp experiments. American Mineralogist, 89, 1078-1086.

Kessel, R., Ulmer, P., Pettke, T., Schmidt, M.W. and Thompson, A.B. (2005) The water-basalt system at 4 to 6 GPa: Phase relations and second critical endpoint in a K-free eclogite at 700 to 1400^{o}C. Earth and Planetary Science Letters, 237, 873-892.

Konzett, J., Rhede, D., and Frost, D.J. (2011) The high PT stability of apatite and Cl partitioning between apatite and hydrous potassic phases in peridotite: an experimental study to 19 GPa with implications for the transport of P, Cl and K in the upper mantle. Contributions to Mineralogy and Petrology, 163, 277-296.

Lassiter, J., and Hauri, E. (1998) Osmium-isotope variations in Hawaiian lavas: evidence for recycled oceanic lithosphere in the Hawaiian plume. Earth and Planetary Science Letters, 164, 483-496.

Le Roex, V., Dick, H.J.B. and Shimizu, N. (2014) Tracking flux melting and melt percolation in supra-subduction peridotites (Josephine ophiolite USA). Contributions to Mineralogy and Petrology, 168, 1064-1086.

Malaspina, N., Hermann, J., Scambelluri, M., and Compagnoni, R. (2006) Multistage metasomatism in ultrahigh-pressure mafic rocks from the North Dabie Complex (China). Lithos, 90, 19-42.

Mallik, A., and Dasgupta, R. (2012) Reaction between MORB-eclogite derived melts and fertile peridotite and generation of ocean island basalts. Earth and Planetary Science Letters, 329-330, 97-108.

Melekhova, E., Schmidt, M.W., Ulmer, P., and Pettke, T. (2007) The composition of liquids coexisting with dense hydrous magnesium silicates at 11–13.5GPa and the endpoints of the solidi in the $MgO–SiO_2–H_2O$ system. Geochimica et Cosmochimica Acta, 71, 3348-3360.

Meltzer, A., and Kessel, R. (2020) Modelling garnet-fluid partitioning in H2O-bearing systems: a preliminary statistical attempt to extend the crystal lattice-strain theory to hydrous systems. Contributions to Mineralogy and Petrology, 175, 80-96.

Putirka, K. (2008) Excess temperatures at ocean islands: Implications for mantle layering and convection. Geology, 36(4).

Qian, S., Salters, V.J.M., McCoy-West, A.J., Wu, J., Rose-Koga, E.F., Nicols, A.R.L., Zhang, L., Zhou, H., and Hoernle, K. (2022) Highly heterogeneous mantle caused by recycling of oceanic lithosphere from the mantle transition zone. Earth and Planetary Science Letters, 593, 117679.

Qiao, J., Zhou, C.-A., Dong, J., Allen, M.B., Yang, L., and Su, L. (2023) Syn- and post-collisional potassic to ultrapotassic alkaline and subalkaline volcanic rocks: Heterogeneous mantle metasomatism beneath the North Qaidam orogenic belt. Lithos, 442, 107081.

Rapp, R.P., Shimizu, N., Norman, M., and Applegate, G. (1999) Reaction between slab-derived melts and peridotite in the mantle wedge: experimental constraints at 3.8 GPa. chemical Geology, 160, 335-356.

Saha, S., Dasgupta, R., and Tsuno, K. (2018) High Pressure Phase Relations of a Depleted Peridotite Fluxed by CO_2-H_2O-Bearing Siliceous Melts and the Origin of Mid-Lithospheric Discontinuity. Geochemistry, Geophysics, Geosystems, 19, 595-620.

Schaffer, A.J., and Lebedev, S. (2013) Global shear speed structure of the upper mantle and transition zone. Geophysical Journal International, 194, 417-449.

Schmidt, M.W., and Poli, S. (1998) Experimentally based water budgets for dehydrating slabs and consequences for arc magma generation. Earth and Planetary Science Letters, 163, 361-379.

Sekine, T., and Wyllie, P.J. (1983) Experimental simulation of mantle hybridization in subduction zones. The Journal of Geology, 91, 511-528.

Smith, C.B., Pearson, D.G., Bulanova, G.P., Beard, A.D., Carlson, R.W., Wittig, N., Sims, K., Chimuka, L. and Muchemwa, E. (2009) Extremely depleted lithospheric mantle and diamonds beneath the southern Zimbabwe Craton. Lithos, 112, 1120-1132.

Sobolev, A.V., Hofmann, A.W., Sobolev, S., V. and Nikogosian, I.K. (2005) An olivine-free mantle source of Hawaiian shield basalts. Nature, 434, 590-597.

Stachel, T., and Harris, J.W. (2008) The origin of cratonic diamonds — Constraints from mineral inclusions. Ore Geology Reviews, 34, 5-32.

Stachel, T., Harris, J.W., Hunt, L., Muehlenbachs, K., and Kobussen, A.F. (2018) Argyle Diamonds: How Subduction Along the Kimberley Craton Edge Generated the World's Biggest Diamond Deposit. In A.T. Davy, C.B. Smith, H. Helmstaedt, A.L. Jaques, and J.J. Gurney, Eds. Geoscience and Exploration of the Argyle, Bunder, Diavik, and Murowa Diamond Deposits, 20.

Stagno, V., and Frost, D.J. (2010) Carbon speciation in the asthenosphere: Experimental measurements of the redox conditions at which carbonate-bearing melts coexist with graphite or diamond in peridotite assemblages. Earth and Planetary Science Letters, 300, 72-84.

Stracke, A. (2012) Earth's heterogeneous mantle: A product of convection-driven interaction between crust and mantle. Chemical Geology, 330, 274-299.

Takahashi, E., and Gao, S. (2015) Experimental Melting Study of Basalt-Peridotite Hybrid Source: Melting model of Hawaiian plume. American Geophysical Union, Fall Meeting 2015AGU.

Thomson, A.R., Walter, M.J., Kohn, S.C., and Brooker, R.A. (2016) Slab melting as a barrier to deep carbon subduction. Nature, 529(7584), 76-79.

Truckenbrodt, J., and Johannes, W. (1999) H_2O loss during piston-cylinder experiments. American Mineralogist, 84(9), 1333-1335.

Truckenbrodt, J., Ziegenbein, D., and Johannes, W. (1997) Redox conditions in piston-cylinder apparatus: The different behavior of boron nitride and unfired pyrophyllite assemblies. American Mineralogist, 82(3-4), 337-344.

Wang, C., Jin, Z., Gao, S., Zhang, J., and Zheng, S. (2010) Eclogite-melt/peridotite reaction: Experimental constrains on the destruction mechanism of the North China Craton. Science China Earth Sciences, 53(6), 797-809.

Wang, C., Liang, Y., Dygert, N., and Xu, W. (2016) Formation of orthopyroxenite by reaction between peridotite and hydrous basaltic melt: an experimental study. Contributions to Mineralogy and Petrology, 171(8-9).

Woodland, A., and O'Neill, H.S.C. (1997) Thermodynamic data for Fe-bearing phases obtained using noble metal alloys as redox sensors. Geochimica et Cosmochimica Acta, 61(20), 4359-4366.

Wyllie, P.J. (1987) Discussion of recent papers on carbonated peridotite, bearing on mantle metasomatism and magmatism. Earth and Planetary Science Letters, 82, 391-397.

Xu, M., Jing, Z., Bajgain, S.K., Mookherjee, M., Van Orman, J.A., Yu, T., and Wang, Y. (2020) High-pressure elastic properties of dolomite melt supporting carbonate-induced melting in deep upper mantle. Proc Natl Acad Sci U S A, 117(31), 18285-18291.

Yaxley, G.M., and Green, D.H. (1998) Reactions between eclogite and peridotite: mantle refertilisation by subduction of oceanic crust. Schweizerische mineralogische und petrographische Mitteilungen, 78(2), 243-255.

Yogodzinski, G.M., Volynets, O.N., Koloskov, A.V., Seliverston, N.I., and Matvenkov, V.V. (1994) Magnesian andesites and the subduction component in a strongly calc-alkaline series at Piip Volcano, far Western Aleutians. Journal of Petrology, 35, 163-204

TABLE 1. Chemical compositions of starting material

	Eclogite (CKB)		Harzburgite (DHRZ)	
wt%	OE-1	OE-2	OE-3	OE-4
SiO_2	49.47	49.33	45.15	45.24
TiO_2	1.63	1.64	-	-
Cr_2O_3	-	-	0.75	0.76
Al_2O_3	15.10	15.08	0.62	0.63
FeO[b]	9.63	9.68	5.64	6.19
MnO	-		0.09	0.09
CaO	10.86	10.86	0.51	0.52
MgO	7.03	7.10	46.20	45.52
Na_2O	2.51	2.55	-	-
K_2O	0.49	0.49	-	-
NiO	-		0.31	0.31
H_2O				
CO_2[b]	3.08-3.11		0.42-0.46	
Total[c]	99.80	99.82	99.74	99.28
Th (ppm)	58	56	-	-
Cs (ppm)	-		35	36
Mg#[c]	0.57	0.57	0.94	0.93
Ca#[d]	0.38	0.38	0.01	0.01

[a] All Fe is expressed as FeO.
[b] The wt% CO_2 was measured via the QTS technique (Dvir and Kessel 2013).
[c] Mg# (molar) = Mg/(Mg+Fe)
[d] Ca# (molar) = Ca/(Ca+Mg+Fe)

This is the peer-reviewed, final accepted version for American Mineralogist, published by the Mineralogical Society of America.
The published version is subject to change. Cite as Authors (Year) Title. American Mineralogist, in press.
DOI: https://doi.org/10.2138/am-2022-8799. http://www.minsocam.org/

TABLE 2. Capsule set up and experimental conditions

Run#	Capsule#	lithology	Harz/Ecl	wt% diamond[a]	Total powder (mg) [b]	wt% H_2O [c]	Rotation time	duration (hr) [d]	$T_{opx\text{-}cpx}$ (^oC) [e]
EHR17	30	Harzburgite	-	16	15.00	10	15 min	21	
EHR18	41	Eclogite	-	20	10.29	9	15 min	20	
EHR19	40	hybrid	0.99	19	13.81	10	static	24	1179
EHR14	35	hybrid	1.05	16	11.74	8	15 min	24	1209
EHR16	38	hybrid	1.03	17	11.42	9	15 sec	21	1262

[a] wt% diamonds – wt% of diamond powder in the system powder + H_2O + CO_2 + diamonds.
[b] wt% H_2O – wt% of H_2O powder in the system powder + H_2O + CO_2.
[c] wt% CO_2 – wt% of CO_2 powder in the system powder + H_2O + CO_2.
[d] Rotation time – the time elapsed between rotations.
[e] Equilibrium temperature calculated based on the Mg-Fe exchange between orthopyroxene and clinopyroxene (Putrika 2008).

This is the peer-reviewed, final accepted version for American Mineralogist, published by the Mineralogical Society of America.
The published version is subject to change. Cite as Authors (Year) Title. American Mineralogist, in press.
DOI: https://doi.org/10.2138/am-2022-8799. http://www.minsocam.org/

TABLE 3. Olivine compositions in this study

	Control		Hybrid	
	Harzburgite	static	15 min	15 sec
Capsule#	30	40	35	38
n[a]	28	10	23	10
SiO_2	41.60(40)[c]	41.18(52)	41.44(40)	41.19(50)
TiO_2	Bdl[d]	0.03(2)	0.07(3)	0.05(3)
Cr_2O_3	0.12(9)	0.14(4)	0.10(6)	0.08(2)
Al_2O_3	0.03(4)	0.06(5)	0.04(4)	0.02(2)
FeO[b]	5.63(67)	6.61(65)	7.54(28)	7.94(54)
CaO	0.02(1)	0.05(5)	0.04(3)	0.04(2)
MgO	52.31(57)	51.59(1.03)	50.11(44)	50.11(63)
MnO	0.09(2)	0.0(3)	0.07(2)	0.04(2)
NiO	0.30(10)	0.32(13)	0.37(5)	0.40(7)
Na_2O	bdl	0.01(1)	0.01(1)	0.02(2)
K_2O	0.01(1)	0.01(1)	bdl	0.01(1)
Total	100.13	100.07	99.79	99.90
Mg#[e]	0.943(7)	0.933(6)	0.922(3)	0.918(6)

[a]Number of analyses throughout the capsule.
[b]All Fe is expressed as FeO
[c]Numbers enclosed in parentheses indicate 1 standard deviation of the last digit quoted, i.e., 41.60(40) should be read as 41.60±0.40.
[d]bdl – below detection limit.
[e]Mg# (molar) = Mg/(Mg+Fe)

This is the peer-reviewed, final accepted version for American Mineralogist, published by the Mineralogical Society of America.
The published version is subject to change. Cite as Authors (Year) Title. American Mineralogist, in press.
DOI: https://doi.org/10.2138/am-2022-8799. http://www.minsocam.org/

TABLE 4. Orthopyroxene compositions in this study

	Control		Hybrid	
	Harzburgite	static	15 min	15 sec
Capsule#	30	40	35	38
n[a]	18	9	37	24
SiO_2	58.48(41)[c]	56.31(1.31)	57.70(57)	57.86(59)
TiO_2	Bdl[d]	0.06(4)	0.14(3)	0.13(2)
Cr_2O_3	0.74(8)	0.49(10)	0.55(16)	0.54(14)
Al_2O_3	1.24(34)	1.39(51)	1.53(42)	1.08(15)
FeO[b]	3.69(24)	4.54(29)	4.79(35)	4.60(42)
CaO	0.20(3)	0.32(6)	0.71(37)	0.51(18)
MgO	36.59(33)	36.16(80)	34.73(19)	35.61(69)
MnO	0.08(2)	0.05(2)	0.03(1)	0.03(2)
NiO	0.11(3)	0.19(6)	0.19(5)	0.14(4)
Na_2O	0.01(1)	0.11(5)	0.15 (4)	0.13(3)
K_2O	bdl	0.01(1)	0.01(1)	0.01(1)
Total	101.14	99.63	100.53	100.64
Mg#[e]	0.946(4)	0.934(4)	0.928(5)	0.932(6)

[a]Number of analyses throughout the capsule.
[b]All Fe is expressed as FeO
[c]Numbers enclosed in parentheses indicate 1 standard deviation of the last digit quoted, i.e., 58.48(41) should be read as 58.48±0.41.
[d]bdl – below detection limit.
[e]Mg# (molar) = Mg/(Mg+Fe)

This is the peer-reviewed, final accepted version for American Mineralogist, published by the Mineralogical Society of America.
The published version is subject to change. Cite as Authors (Year) Title. American Mineralogist, in press.
DOI: https://doi.org/10.2138/am-2022-8799. http://www.minsocam.org/

TABLE 5. Clinopyroxene compositions in this study

Capsule#	static	Hybrid 15 min	15 sec
	40	35	38
n[a]	4	22	18
SiO_2	54.85(33)[c]	54.58(56)	54.90(35)
TiO_2	0.03(2)	0.35(6)	0.26(5)
Cr_2O_3	1.42(53)	0.99(60)	0.62(41)
Al_2O_3	1.40(27)	3.00(35)	2.10(38)
FeO[b]	2.00(24)	2.55(22)	3.01(31)
CaO	20.02(88)	19.07(58)	18.96(79)
MgO	18.45(1.19)	17.66(52)	18.48(81)
MnO	0.04(5)	0.01(1)	0.02(2)
NiO	0.04(2)	0.06(3)	0.05(3)
Na_2O	2.15(33)	2.62(33)	1.97(33)
K_2O	0.04(3)	0.01(1)	0.02(1)
Total	100.44	100.89	100.38
Mg#[d]	0.943(4)	0.924(5)	0.916(7)

[a]Number of analyses throughout the capsule.
[b]All Fe is expressed as FeO
[c]Numbers enclosed in parentheses indicate 1 standard deviation of the last digit quoted, i.e., 54.85(33) should be read as 54.85±0.33.
[d]Mg# (molar) = Mg/(Mg+Fe)

This is the peer-reviewed, final accepted version for American Mineralogist, published by the Mineralogical Society of America.
The published version is subject to change. Cite as Authors (Year) Title. American Mineralogist, in press.
DOI: https://doi.org/10.2138/am-2022-8799. http://www.minsocam.org/

TABLE 6. Garnet compositions in this study

	Control		Hybrid					
Capsule	Harzburgite	Eclogite	40		35		38	
			Harzburgite	Eclogite	Harzburgite	Eclogite	Harzburgite	Eclogite
N[a]	28	10	6	8	5	5	6	8
SiO_2	42.19(24)[c]	42.05(48)	43.44(36)	42.05(36)	42.24(80)	40.19(50)	41.83(97)	41.22(14)
TiO_2	bdl	0.56(16)	0.17(19)	0.98(19)	0.87(14)	0.59(30)	0.96(23)	0.69(19)
Cr_2O_3	3.19(78)	0.01(1)	0.75(4)	0.05(4)	4.78(54)	0.17(5)	3.04(1.07)	0.23(27)
Al_2O_3	22.27(67)	23.80(43)	23.40(44)	23.52(44)	19.63(90)	24.42(61)	19.93(1.22)	22.79(44)
FeO[b]	6.27(18)	13.61(27)	9.28(25)	11.36(25)	6.14(1.02)	8.85(49)	7.23(61)	8.33(25)
CaO	2.28(20)	8.20(39)	4.85(60)	9.77(60)	6.64(98)	6.92(1.03)	6.35(69)	6.34(49)
MgO	23.15(30)	12.67(42)	19.15(42)	13.07(42)	19.67(1.23)	17.64(94)	19.29(1.12)	18.36(30)
MnO	0.31(3)	0.02(2)	N.A.[e]	0.03(2)	0.07(4)	0.07(1)	0.01(2)	0.08(2)
NiO	0.02(2)	0.01(1)	N.A.[e]	0.01(1)	0.03(3)	0.02(2)	0.01(2)	0.01(2)
Na_2O	0.01(1)	0.18(4)	0.05(14)	0.23(14)	0.18(5)	0.10(1)	0.11(3)	0.07(1)
K_2O	Bdl[d]	0.01(1)	bdl	bdl	0.01(1)	0.01(1)	0.01(2)	0.01(1)
Total	99.69	101.13	101.08	101.09	100.26	99.89	98.78	98.12
Mg#[f]	0.868(3)	0.624(8)	0.784(5)	0.672(8)	0.850(28)	0.780(18)	0.826(19)	0.797(6)

[a]Number of analyses throughout the capsule.
[b]All Fe is expressed as FeO
[c]Numbers enclosed in parentheses indicate 1 standard deviation of the last digit quoted, i.e., 42.19(24) should be read as 42.19±0.24.
[d]bdl – below detection limit.
[e]N.A. – Not analyzed.
[f]Mg# (molar) = Mg/(Mg+Fe)

This is the peer-reviewed, final accepted version for American Mineralogist, published by the Mineralogical Society of America.
The published version is subject to change. Cite as Authors (Year) Title. American Mineralogist, in press.
DOI: https://doi.org/10.2138/am-2022-8799. http://www.minsocam.org/

TABLE 7. Fluid and melt compositions in this study

	Control		Hybrid		
	Harzburgite	Eclogite	static	15 min	15 sec
Capsule#	30	41	40	35	38
N[a]	13	14	7	5	6
SiO_2	13.41(71)[c]	50.03(2.45)	53.13(91)	27.69 (82)	33.97(1.22)
TiO_2	0.011(1)	1.64(13)	1.07(24)	1.64(11)	1.95(20)
Cr_2O_3	0.08(2)	bdl	0.02(2)	0.02(1)	0.008(5)
Al_2O_3	1.11(16)	12.78(1.95)	8.78(1.13)	8.06(62)	6.20(62)
FeO[b]	3.17(1.21)	6.11(1.33)	3.77(77)	4.83(42)	6.93(96)
CaO	3.34(30)	10.50(38)	8.88(2.66)	5.44(34)	8.45(75)
MgO	13.28(1.28)	5.39(1.00)	7.62(42)	14.58(69)	10.79(1.18)
MnO	0.08(2)	bdl	0.009(0)	0.04(1)	0.03(1)
NiO	0.01(1)	bdl	bdl	0.007(1)	0.012(7)
Na_2O	bdl[d]	3.98(1.12)	4.72(45)	5.52(14)	5.25(3.18)
K_2O	bdl	0.46(6)	0.73(21)	1.54(19)	1.24(20)
H_2O	62.63(2.67)	6.82(87)	15.52(2.10)	25.20(1.48)	20.42(1.75)
CO_2	2.86(12)	2.28(29)	2.76(37)	5.43(32)	4.74(41)
Total	100.00	100.00	100.00	100.00	100.00
Mg#[e]	0.88(3)	0.61(1)	0.78(3)	0.84(18)	0.75(2)
Ca#[f]	0.11(2)	0.46(5)	0.39(8)	0.18(1)	0.30(5)

[a]Number of analyses throughout the capsule.
[b]All Fe is expressed as FeO
[c]Numbers enclosed in parentheses indicate 1 standard deviation of the last digit quoted, i.e., 42.19(24) should be read as 42.19±0.24.
[d]bdl – below detection limit.
[e]Mg# (molar) = Mg/(Mg+Fe)
[f]Ca# (molar) = Ca/(Ca+Mg+Fe)

This is the peer-reviewed, final accepted version for American Mineralogist, published by the Mineralogical Society of America.
The published version is subject to change. Cite as Authors (Year) Title. American Mineralogist, in press.
DOI: https://doi.org/10.2138/am-2022-8799. http://www.minsocam.org/

TABLE 8. Modal phase abundance

	Control		Hybrid		
	Harzburgite	Eclogite	static	15 min	15 sec
Capsule#	30	41	40	35	38
Olivine	0.58(2)[a]	–	0.16(2)	0.08(3)	0.11(4)
opx	0.25(2)	–	0.17(5)	0.31(5)	0.26(6)
cpx	–[b]	–	0.04(3)	0.13(4)	0.08(6)
Garnet(ecl)	–	0.24(7)	0.42(7)	0.28(10)	0.27(34)
Garnet(Hrz)	0.01(1)	–	0.02(8)	0.03(13)	0.03(38)
Fluid	0.15(2)	–	–	–	–
Melt	–	0.76(7)	0.19(3)	0.17(2)	0.25(9)

[a]Numbers enclosed in parentheses indicate 1 standard deviation of the last digit quoted, i.e., 0.58(2) should be read as 0.58±0.2.
[b] – indicates absent from the run product assemblage.

This is the peer-reviewed, final accepted version for American Mineralogist, published by the Mineralogical Society of America.
The published version is subject to change. Cite as Authors (Year) Title. American Mineralogist, in press.
DOI: https://doi.org/10.2138/am-2022-8799. http://www.minsocam.org/

Fig. 1

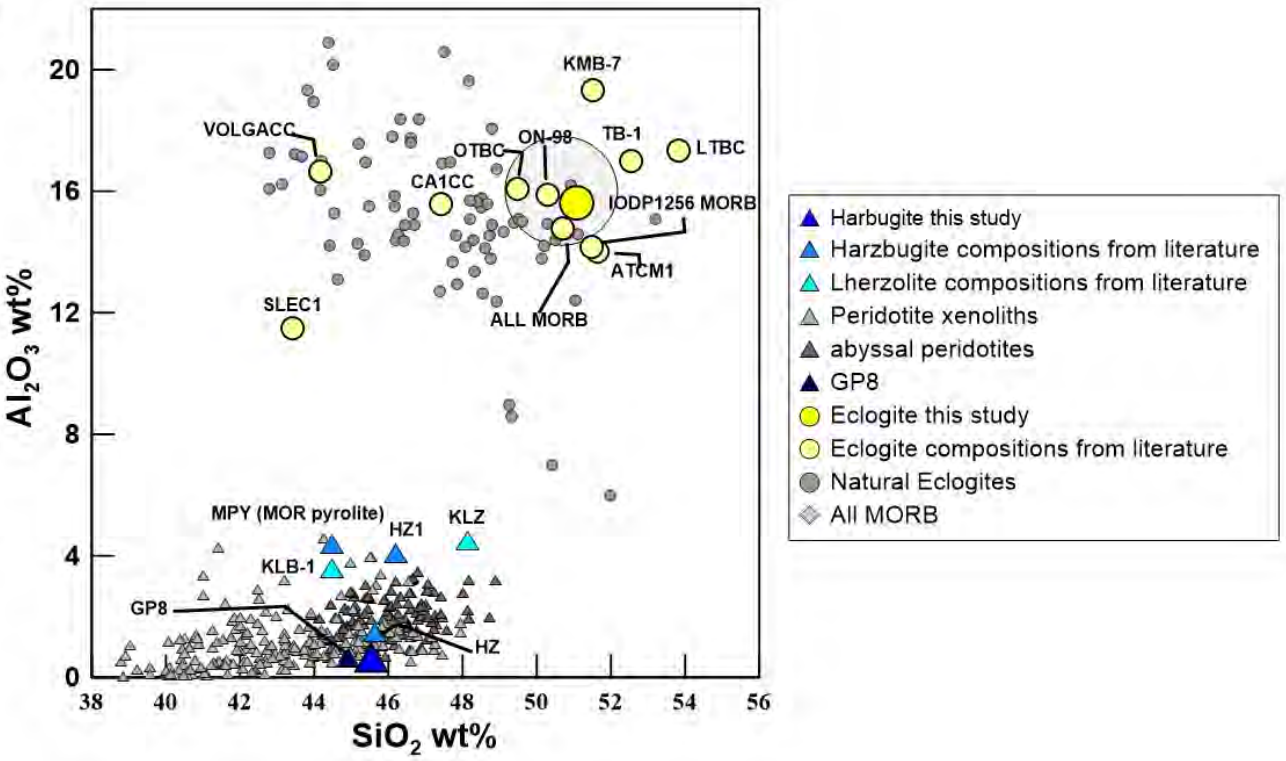

This is the peer-reviewed, final accepted version for American Mineralogist, published by the Mineralogical Society of America.
The published version is subject to change. Cite as Authors (Year) Title. American Mineralogist, in press.
DOI: https://doi.org/10.2138/am-2022-8799. http://www.minsocam.org/

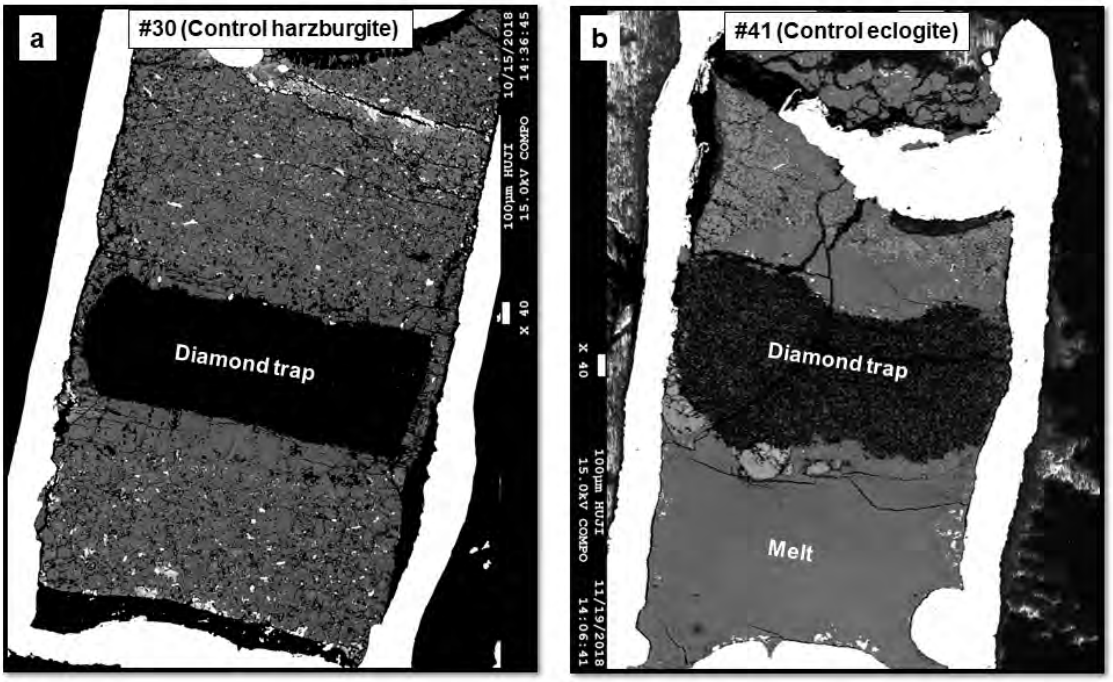

Fig. 2

This is the peer-reviewed, final accepted version for American Mineralogist, published by the Mineralogical Society of America.
The published version is subject to change. Cite as Authors (Year) Title. American Mineralogist, in press.
DOI: https://doi.org/10.2138/am-2022-8799. http://www.minsocam.org/

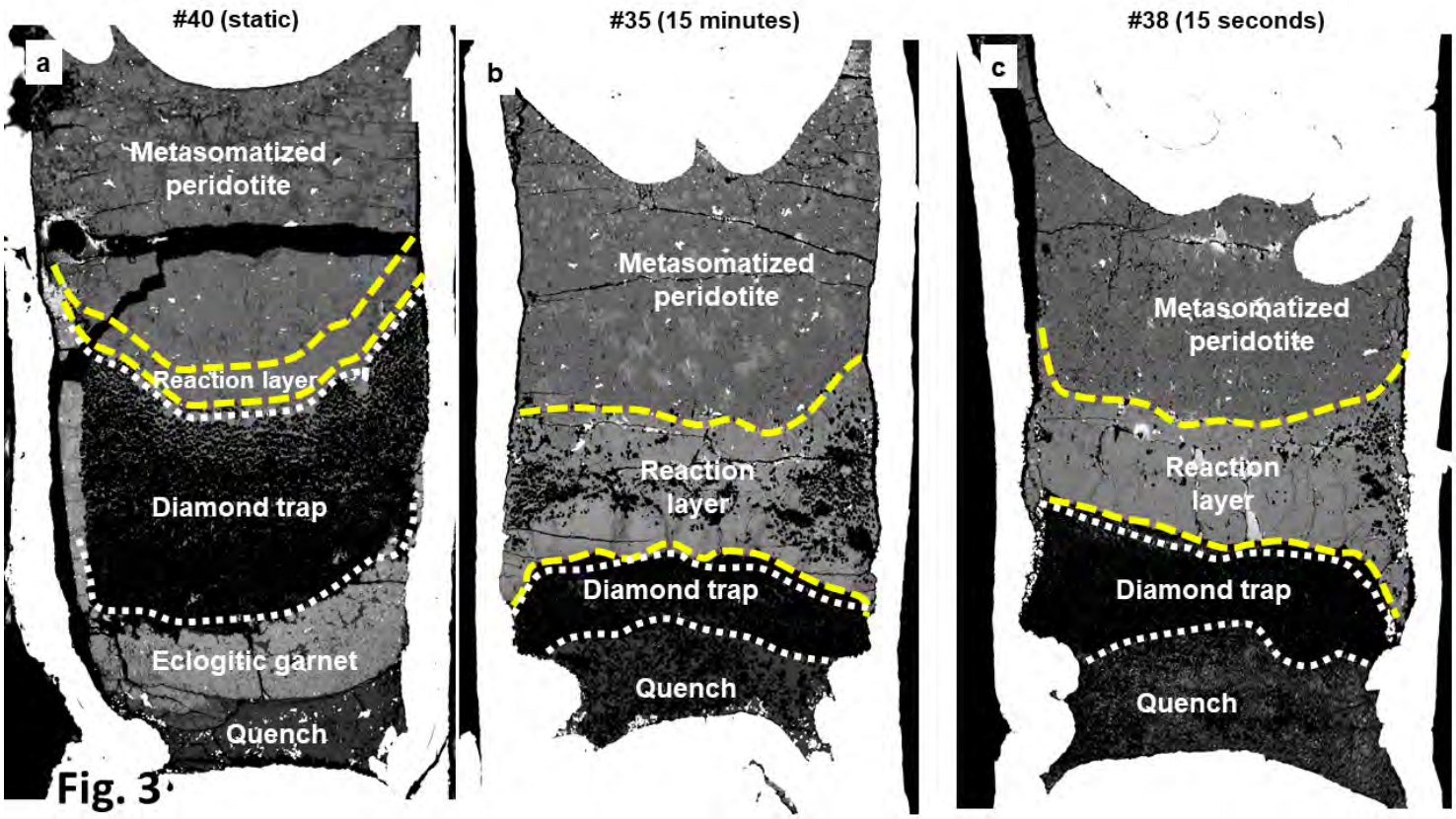

Fig. 3

This is the peer-reviewed, final accepted version for American Mineralogist, published by the Mineralogical Society of America.
The published version is subject to change. Cite as Authors (Year) Title. American Mineralogist, in press.
DOI: https://doi.org/10.2138/am-2022-8799. http://www.minsocam.org/

Fig. 4

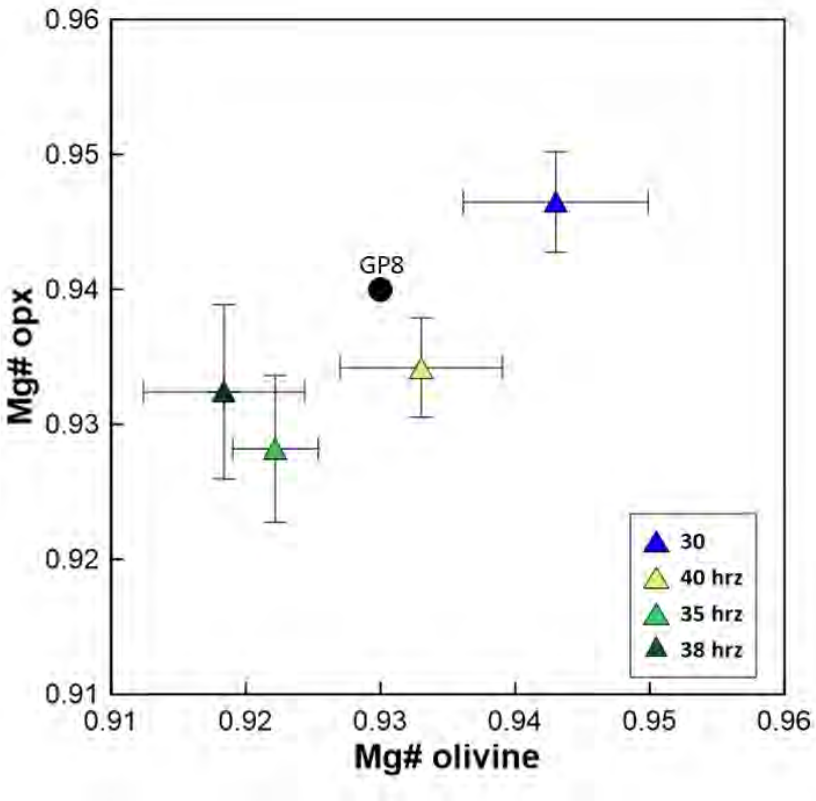

This is the peer-reviewed, final accepted version for American Mineralogist, published by the Mineralogical Society of America.
The published version is subject to change. Cite as Authors (Year) Title. American Mineralogist, in press.
DOI: https://doi.org/10.2138/am-2022-8799. http://www.minsocam.org/

Fig. 5

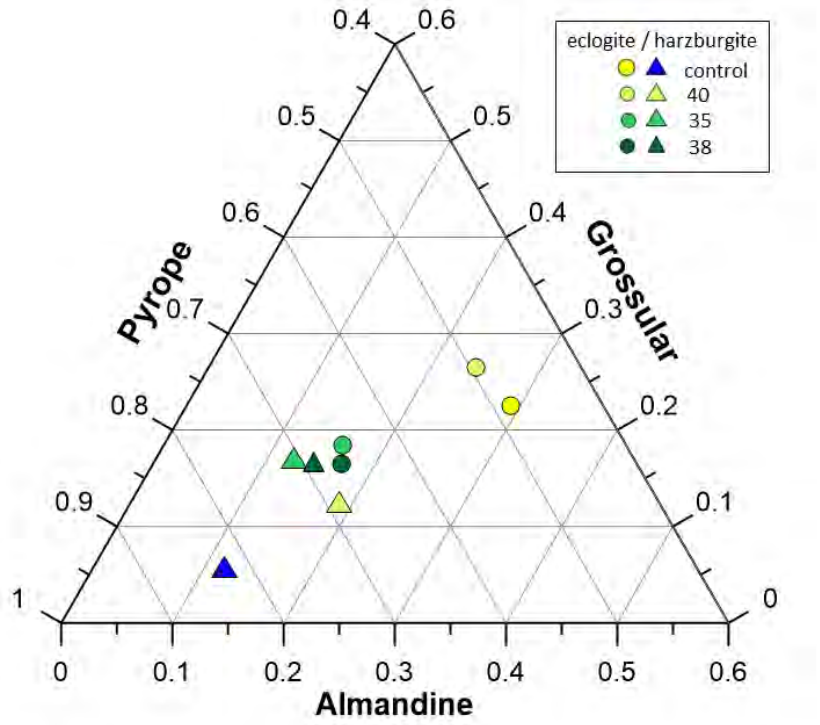

This is the peer-reviewed, final accepted version for American Mineralogist, published by the Mineralogical Society of America.
The published version is subject to change. Cite as Authors (Year) Title. American Mineralogist, in press.
DOI: https://doi.org/10.2138/am-2022-8799. http://www.minsocam.org/

Fig. 6

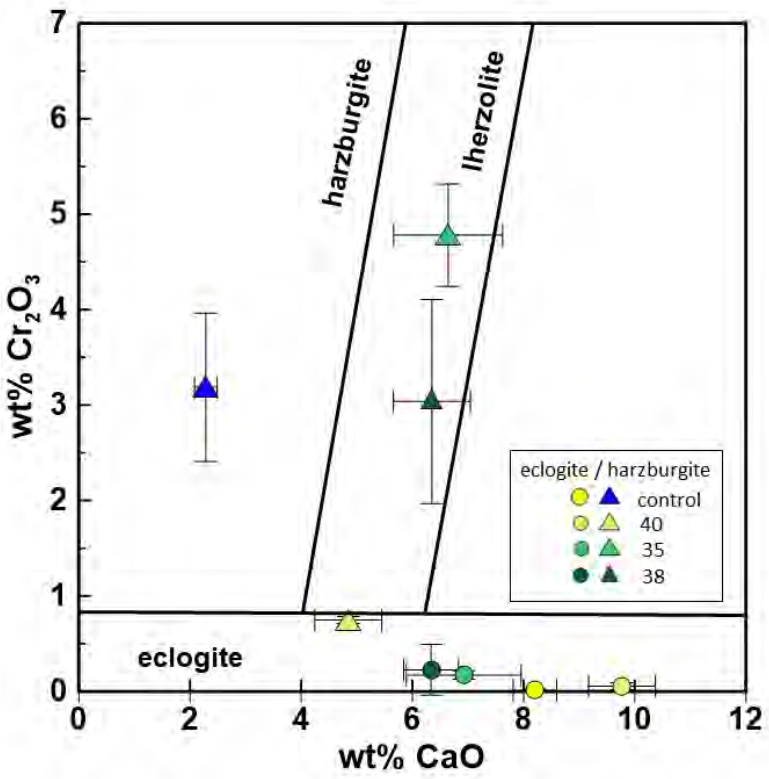

This is the peer-reviewed, final accepted version for American Mineralogist, published by the Mineralogical Society of America.
The published version is subject to change. Cite as Authors (Year) Title. American Mineralogist, in press.
DOI: https://doi.org/10.2138/am-2022-8799. http://www.minsocam.org/

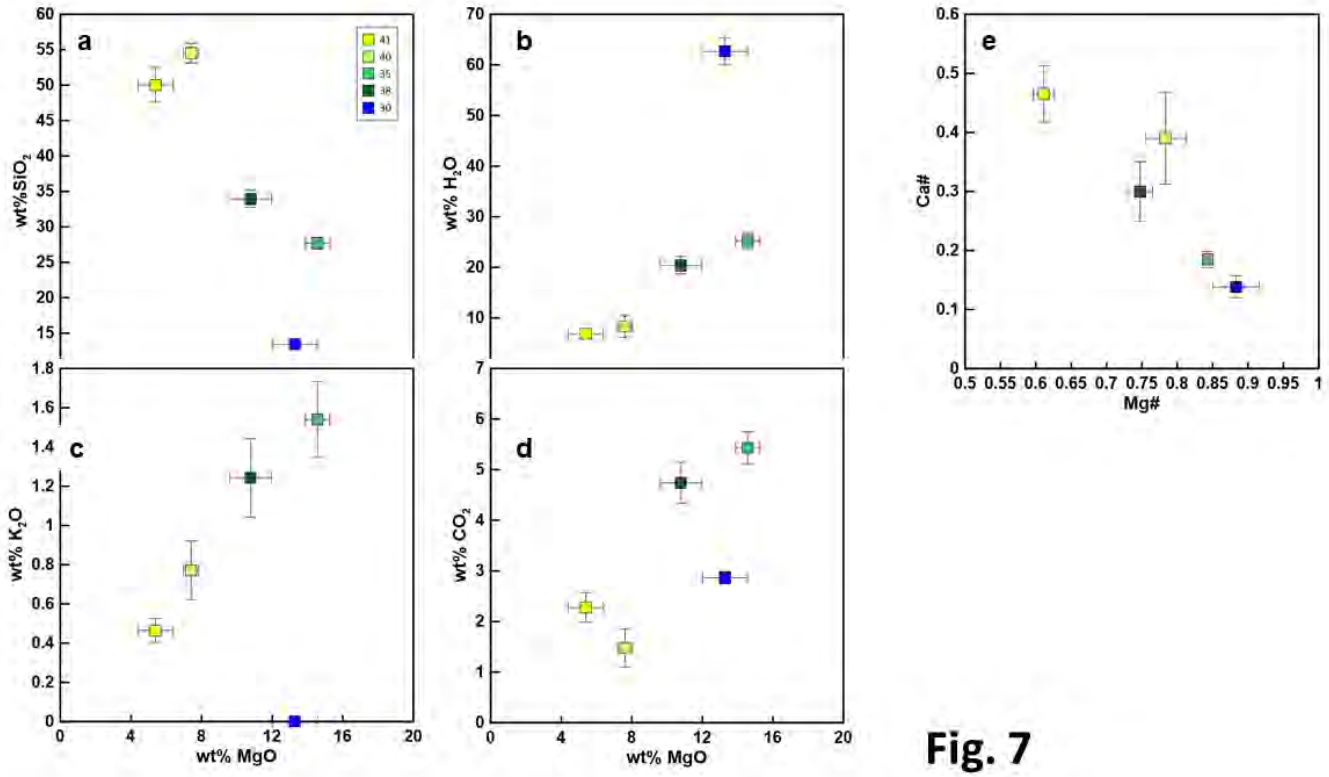

Fig. 7

This is the peer-reviewed, final accepted version for American Mineralogist, published by the Mineralogical Society of America.
The published version is subject to change. Cite as Authors (Year) Title. American Mineralogist, in press.
DOI: https://doi.org/10.2138/am-2022-8799. http://www.minsocam.org/

Fig. 8

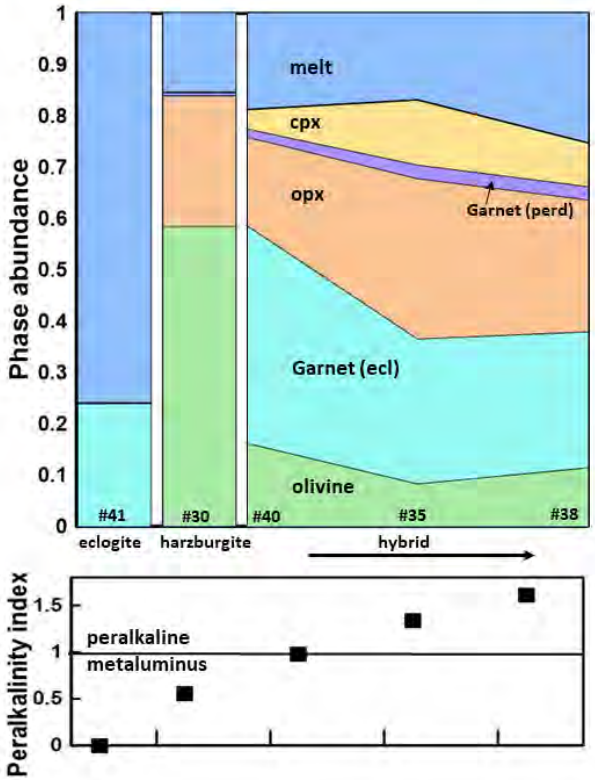

This is the peer-reviewed, final accepted version for American Mineralogist, published by the Mineralogical Society of America.
The published version is subject to change. Cite as Authors (Year) Title. American Mineralogist, in press.
DOI: https://doi.org/10.2138/am-2022-8799. http://www.minsocam.org/

Fig. 9